Available online at www.sciencedirect.com
ScienceDirect
Polymer 48 (2007) 7672–7678
polymer
www.elsevier.com/locate/polymer

QSAR model for ethylene polymerisation catalysed by supported bis(imino)pyridine iron complexes

V.L. Cruz [a,*], J. Martinez [b], J. Martinez-Salazar [a], J. Ramos [a], M.L. Reyes [c], A. Toro-Labbe [b], S. Gutierrez-Oliva [b]

[a] *Instituto de Estructura de la Materia, CSIC, Serrano, 113bis, E-28006 Madrid, Spain*
[b] *Laboratorio de Química Teorica Computacional, Facultad de Quimica, Pontificia Universidad Catolica de Chile, Casilla 306, Correo 22, Santiago, Chile*
[c] *Centro de Tecnología Repsol-YPF, Carretera de Extremadura NV, Km 18, E-28931 Madrid, Spain*

Received 25 July 2007; received in revised form 2 November 2007; accepted 2 November 2007
Available online 12 November 2007

Abstract

We present a quantitative structure–activity relationship study performed over a set of bis(imino)pyridine iron catalyst used for olefin polymerisation. The experimental results were previously obtained by our research group. The structural variability of this catalyst set is mainly focused on the substituents of the aryl rings. We managed to find a statistically robust model which correlates the experimentally determined polymer's molecular weight with the steric and electrostatic fields. As a result the main contribution comes from the steric contribution which amounts up to 75% of the model. The predictive capability of the model was successfully probed with a test set of catalyst reported in the literature by other research group.

Keywords: Bis(imino)pyridine iron catalyst; 3D-QSAR; Ethylene polymerisation

1. Introduction

In 1998, Brookhart et al. [1] and Gibson et al. [2] reported for the first time the use of a bis(imino)pyridine iron catalyst for ethylene polymerisation. It is well documented that bis-(imino)pyridine iron catalyst can be considered as one of the most promising industrial catalytic systems developed in the last decade [1,3–10]. However, the quantitative aspects of the influence of ligand substituents on the performance of highly active iron catalyst for ethylene polymerisation still remain largely unknown. Then, some of our recent experimental and computational efforts have been addressed towards the role of the ligand substituents on the ethylene polymerisation for various catalysts involving late transition metal [11–13].

Generally speaking, a focused target in the polymerisation catalysis is the efficient control of the activity and the molecular weight. This is experimentally carried out by the trial-error selection of the optimal experimental conditions and convenient ancillary ligands on the catalysts, among hundreds of potential candidates. Thus the bis(imino)pyridine ligand offers great opportunities for fine-tuning of the catalytic properties due to the well-defined environment on the ligand. In this line several experimental works have empirically explored the steric–electronic influence of different groups on the imino aryl rings [14–16]. However, the synthesis and screening of potential candidates can be extremely expensive and laborious. Here, the use of quantitative structure–activity relationship (QSAR) technique can be of considerable help to guide the experimental design with a final reduction in the number of experiments. Indeed, QSAR is considered as an essential tool for the design of new drugs in the medicinal chemistry field [17].

This successful application of 3D-QSAR methodologies in drug design [18] has stimulated us to apply them for the study of single site polymerisation catalysis [19,20]. Then, various partially successful attempts to improve the catalyst activity by systematic ligand modifications have been described [3–5].

* Corresponding author. Tel.: +34 915616800.
E-mail address: victor.cruz@iem.cfmac.csic.es (V.L. Cruz).

0032-3861/$ - see front matter © 2007 Elsevier Ltd. All rights reserved.
doi:10.1016/j.polymer.2007.11.011

One of the main criticisms raised against the usage of 3D-QSAR is the inclusion of a high number of variables used to correlate with a few dependent variables. However, it should be taken into account that these variables are no longer independent and cannot be used as in Multivariate Linear Correlation techniques. The development of statistical techniques such as Partial Least Squares (PLS) helps to solve this situation allowing one to derive true independent variables (latent variables) which, at the same time, are used for the fitting procedure. Other criticism commonly made by researchers in the homogeneous catalysis field for the usage of QSAR tools concerns the complexity of the real system in comparison with the model used in the QSAR analysis. Of course, this is the fundamental drawback inherent to any simulation or theoretical methodology. Furthermore, there is an additional point of debate with the application of QSAR, i.e., the calculated descriptors are directly correlated with experimental values. In general, many factors other than molecular structure might influence the action of any drug or catalyst. However, careful and systematic experiments using well controlled experimental conditions can be performed to isolate the structural effects as much as possible. The validity of this approach has been demonstrated by the numerous successful cases in the drug design field [18]. The area of homogeneous catalysis should not exhibit, in principle, further complications. Among the different QSAR tools, three-dimensional quantitative structure–activity relationship (3D-QSAR) [18] is one of the most useful methodologies due to its capability to capture the main structural features associated to a particular biological response.

In this work, we report a 3D-QSAR analysis applied to a set of iron-based catalysts used in the polymerisation of ethylene and carried out in our research collaborative group. We describe the models obtained as well as the results of their predictive capability when applied to a set of compounds reported by other research group [21].

2. Methods

2.1. Polymerisation experiments

The ethylene polymerisation experiments were carried out with heterogeneous catalysts (supported on SiO_2–MAO, 15 wt% Al) in heptane, to 4 bar, in the presence of TIBA like ''scavenger'', at 70 °C. Polymer molecular weights were determined by GPC (Waters 150C Plus) in 1,2,4-trichlorobenzene at 145 °C.

The catalyst set corresponds to the general structure depicted in Scheme 1. In Table 1 the polymerisation activities for the different catalysts are tabulated together with the molecular weight and polydispersity index of the synthesized polymers.

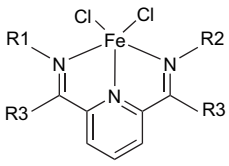

Scheme 1.

2.2. Molecular modelling

For each compound in Table 1, geometry optimization at B3LYP [22]/LANL2DZ [23] was performed using the Gaussian 03 package [24]. We calculated electrostatic charges by fitting the electrostatic potential to nuclear positions according to the CHELPG scheme [25]. Steric and electrostatic 3D fields are calculated using the CoMFA method through the interaction between each catalyst and a probe atom. The probe atom needs to have specific charge and steric properties to permit the evaluation of the interaction energy at each particular point of the grid [26]. The probe atom selected was an sp^3 C atom with a −1 point charge. This atom corresponds to atom C(3) in the Tripos Force Field [27], which was used to calculate Van der Waals (steric) interactions. The value for the probe atom charge was selected such as to represent the effect of the electrostatic nature of either the ethylene or the anionic cocatalyst.

2.3. CoMFA details

All the reported 3D-QSAR analyses were carried out with the CoMFA module [28] implemented in the SYBYL 7.2 package [29].

2.3.1. Alignment rule

It is essential in 3D-QSAR to align all the structures in a common framework in order to make it possible the comparison between all the tested catalysts [26]. In this study the catalyst molecules were aligned in such a way that every compound presented similar orientations. For this task the iron atom and the three coplanar N atoms of the iminopyridine ligand were selected. The resulting alignment is shown in Fig. 1 along with the cubic region used to calculate the molecular fields. Among the various grid spacings tried, the best results were obtained with a lattice spacing of 1.0 Å. This resolution is considered as the optimum value since a higher precision in the evaluation of the 3D field would result in an increase in the so-called ''brown noise'' caused by the grid size sensitivity of the statistical technique used to generate the models [30].

2.3.2. PLS analysis

Partial Least Squares (PLS) [31] analyses were performed for different combinations of field descriptors. PLS calculations with any combination of fields were carried out using the so-called autoscaling, where each field is scaled to have unit value variance. This autoscaling is performed dividing the field value at each point by the standard deviation (SD) of that field calculated over all points. The effect is to assign to each variable the same prior importance in the analysis. Leave one out (LOO) [32] crossvalidated PLS analysis was initially performed to determine both the robustness of the statistical models and the optimal number of components. This

Table 1
Experimental data

Catalyst	R1	R2	R3	Activity[a]	M_w[b]	PDI
1	2,6-Me_2–Ph	2,6-Me_2–Ph	Me	2405	269	11.9
2	2,4,6-Me_3–Ph	2,4,6-Me_3–Ph	Me	2247	362	19.1
3	2,4,6-Me_3–Ph	2-Me–Ph	Me	6797	126	60
4	2,4,6-Me_3–Ph	2,4,6-Me_3–Ph	$-(CH_2)_3-OSiMe_2{}^tBu$	5030	237	13.3
5	2,4,6-Me_3–Ph	2,4,6-Me_3–Ph	$-(CH_2)_4-OSiMe_2{}^tBu$	1694	332	15.9
6	2,4,6-Me_3–Ph	2-Et–Ph	Me	2768	186	34.8
7	2-Me–Naph	2-Me–Naph	Me	5798	55	6.2
8	2,4,6-Me_3–Ph	2-Me–Naph	Me	1931	182	12.5
9	2,4,6-Me_3–Ph	Naph	Me	3466	73	24.7
10	2,4,6–Me_3–Ph	5,6,7,8–H_4–Naph	Me	2050	25	10.6
11	2,4,6–Me_3–Ph	2,4,6–Me_3–Ph	$-(CH_2)_3-OSiEt_3$	2479	282	13.7
12	2,4,6–Me_3–Ph	2,5–Me_2–Ph	Me	9753	133	50.3
13	2,4,6–Me_3–Ph	2,4,6–Me_3–Ph	$-(CH_2)_3-OSiEt_2{}^iPr$	3450	509	26.9
14	2,4,6–Me_3–Ph	2–Ph–Ph	Me	707	152	25.0
15	2-Cl–4,6-Me_2–Ph	2-Cl–4,6–Me_2–Ph	Me	4615	72	6.8
16	4-Br–2,6-Me_2–Ph	4-Br–2,6-Me_2–Ph	Me	4491	297	19.3
17	2-Cl–6-Me–Ph	2-Cl–6-Me–Ph	Me	3135	111	7.7
18	2-Me–Naph	2-Me–Naph	Bu	5310	146	8.3
19	2-Me–6-^{i}Pr–Ph	2-Me–6-^{i}Pr–Ph	Me	1822	722	20.2

[a] kg PE/((mol Fe) bar h).
[b] kg/mol.

can be achieved by examining the Predictive Residual Sum of Squares (PRESS) and the crossvalidated regression coefficient (q^2) as guidelines. The q^2 statistics is defined as

$$\mathrm{PRESS} = \sum_{i=1}^{N} \left(Y_{\mathrm{obs},i} - Y_{\mathrm{pred},i}\right)^2 \quad (1)$$

$$q^2 = 1 - \mathrm{PRESS}/\mathrm{SSD} \quad (2)$$

where $Y_{\mathrm{obs},i}$ and $Y_{\mathrm{pred},i}$ are, respectively, the actual and predicted dependent variables and SSD is the sum of the squared deviations of each dependent variable from the mean of all dependent variables. It has been estimated by some authors [33] that a q^2 value greater than 0.3 has a 95% confidence limit. The usual practice in drug design is to consider valid a model with q^2 greater than 0.5, i.e., half way between perfect predictions ($q^2 = 1.0$) and no prediction at all ($q^2 = 0.0$). The optimum number of components was determined by minimizing PRESS while maximizing q^2 values. Whenever the increase in q^2 with the consideration of an additional component was less than 5%, the model with fewer components was selected. Addition of more components improves the fitting statistics but it introduces two disadvantages: on one hand, it complicates the model and on the other it makes the model to lose its predictive ability. Finally, subsequent non-crossvalidated PLS analysis was carried out for the optimum number of components to obtain a final model.

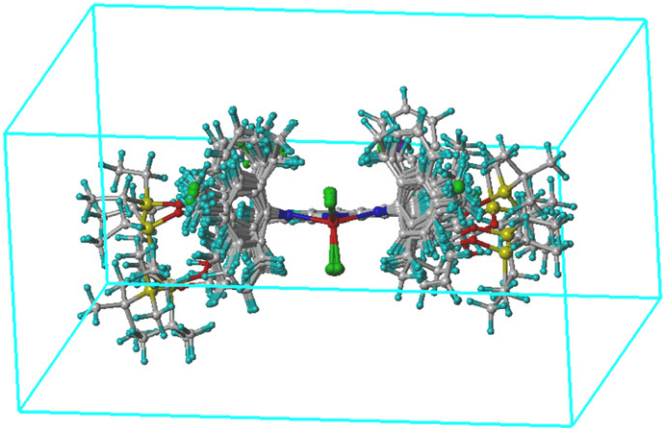

Fig. 1. Resulting alignment and cubic region used to calculate the structural descriptors.

3. Results

In this section the models obtained after application of the chemometric tools described above are discussed in detail. Prior to this, in the first subsection, we present a conformational study to explain the selection of geometries considered in this work.

First of all, it is convenient to clarify some aspects respect to the model used in the CoMFA study. The active species corresponding to this catalytic system still remains unclear. For this reason we decided to consider the dichloride precursors. Although the details corresponding to the influence of the active species structure might be lost, it is worthwhile to study the effect of other structural descriptors on the polymerisation behaviour that could be independent of the nature of the active species. For example the catalyst–cocatalyst interaction is mainly driven by the nature of the ligand substituents around the active centre while the electronic characteristics of the centre itself are by far less important [34].

However, the cocatalyst has not been explicitly included in the model mainly for two reasons. On one hand the precise chemical structure of MAO is still uncertain. On the other hand, it is assumed that the same kind of interaction between

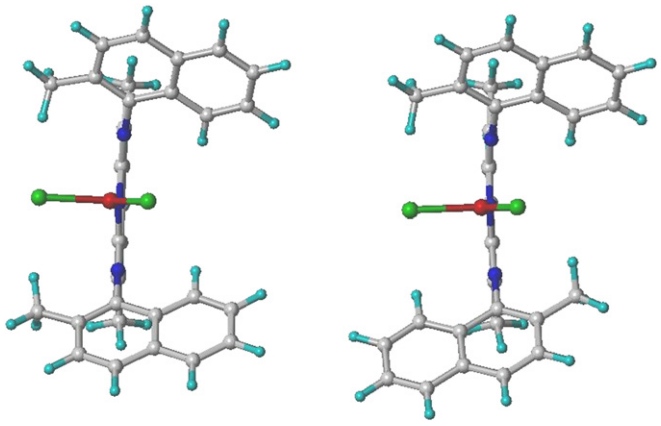

Fig. 2. Atropisomers corresponding to catalyst **7**.

catalyst and MAO will take place in every case, so the inclusion of information about the cocatalyst structure would introduce more noise than signal in the model degrading its statistical significance. In order to evaluate the intermolecular interactions we have selected two descriptors, i.e., the steric and the electrostatic fields [35]. In the following sections we present a detailed description of the main characteristics of the model and discuss the results of its predictive capability.

3.1. Conformational analysis

Some compounds in the training set have the possibility of alternative conformations considering the substituents of the aryl groups. Fig. 2 shows the two alternative atropisomers "*cisoid*" or "*transoid*" with respect to the iminopyridine plane, for catalyst **7**.

In Table 2 we collected the B3LYP energy calculated for the two possible atropisomers of those catalysts showing this isomerization. In general, the energy difference between both conformers is small (around 1 kcal/mol) except for catalyst number **19**. The experimental observation indicates a 1:1 mixture for all catalysts in the set except catalyst **19** where a pure isomer can be isolated but cannot be experimentally determined. The theoretical result allows one to assign the *trans* atropisomer to this catalyst. For the remaining analysis, we considered both conformers to yield the same molecular weight because they are able to coexist at temperatures at which the experiments were performed.

3.2. PLS models

Only one CoMFA model was found to be statistically significant and robust. The model correlates the polymer molecular weight with both the steric and electrostatic fields. We have not been able to obtain a suitable model for the polymerisation activity. We suspect that polymerisation activity is essentially influenced by the nature of active species of the catalyst. Therefore, it would be probably necessary to take into account the nature of the active species to search for correlations between structural descriptors and polymerisation activity.

Table 2
Energy difference in kcal/mol between atropisomers

Catalyst	**7**	**15**	**17**	**18**	**19**
$\Delta E = E_{cis} - E_{trans}$	1.11	−1.79	−1.23	−0.22	3.77

We considered several grid spacing and the best results were obtained with a value of 1 Å. Finer grids resulted in slightly poorer correlation coefficients, most probably due to the introduction of additional noise instead of signal in the descriptor set, as it was previously mentioned.

The best model was obtained with a combination of steric and electrostatic descriptors, i.e., the classical CoMFA field.

The crossvalidated correlation coefficient q^2 was 0.634, with a Standard Error of Prediction of 0.225 for three components. This q^2 value (greater than 0.5) indicates that we have obtained a good predictive model, in accordance with the usual practice in the 3D-QSAR field.

The QSAR model is better depicted in the form of 3D isosurfaces showing the values of the multiplication of standard deviation (stdv) by the QSAR coefficient (coeff) at each point. This field gives information on the salient features of the model, specified by the magnitude of the QSAR coefficients, scaled by the variability associated at each grid point, specified by the standard deviation [36].

In Fig. 3, the stdv × coeff field is shown for the steric contribution to the model. The most positive values of the field are represented as green areas. In these regions, an increase in steric hindrance will be beneficial for obtaining high molecular weights. On the contrary, the yellow areas indicate that steric hindrance will be detrimental for this property.

As can be seen, the regions of positive contributions (green areas in Fig. 3) are located around the *re* face (monomer frontside attack). It is in this face where the termination processes by chain transfer mechanism to the monomer take place, while in the *si* face (backside attack) only chain propagation occurs [37,38]. Steric hindrance on the *re* face is expected to reduce the probability of termination processes, thus resulting in higher molecular weights. Let us analyse another argument given in terms of catalyst–cocatalyst interaction. It is generally accepted that olefin complexation is favoured by catalyst–cocatalyst separation, which provides enough room for the olefin molecule to coordinate the active site. The weaker the ion pair interaction, the easier the olefin approach. In view of the location of the positive steric regions around the active centre the model supports this argument as well. An increase in the steric field in those areas can contribute to ion pair separation, so weakening this interaction. Thus, both theoretical arguments are in consonance with results derived from the QSAR model.

On the other hand, the electrostatic field model shows a congruent image to that found for the steric model. This model is depicted in Fig. 4. The red areas correspond to negative values of the coefficients in the QSAR model. Due to the biphasic nature of the electrostatic field, these values can be associated to locations where an increase in negative charge will be beneficial for getting higher molecular weights. We interpret this result in terms of catalyst–cocatalyst interaction. It is interesting

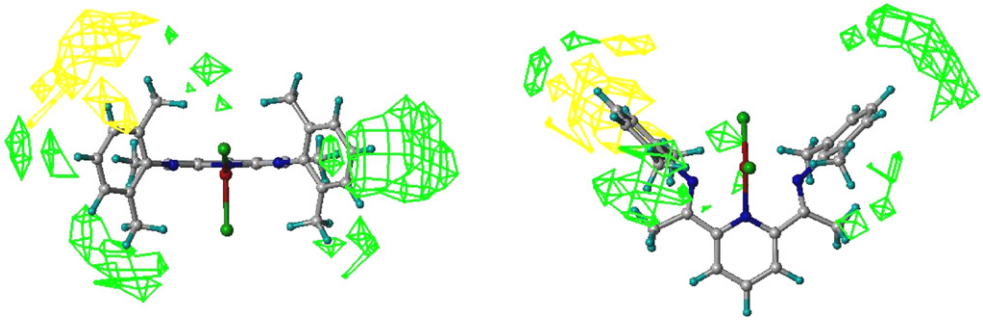

Fig. 3. Steric stdv × coeff field contoured at the highest contribution (green) and lowest contribution (yellow) graphed onto catalyst **1**. Left image corresponds to an equatorial viewpoint. Right image is an axial viewpoint. (For interpretation of the references to color in this figure legend, the reader is referred to the web version of this article.)

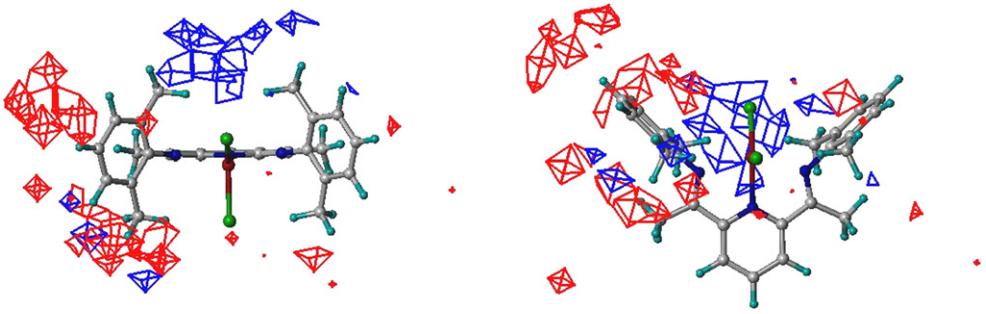

Fig. 4. Electrostatic stdv × coeff field contoured at the highest contribution (blue) and lowest contribution (red) graphed onto catalyst **1**. Left image corresponds to an equatorial viewpoint. Right image is an axial viewpoint. (For interpretation of the references to color in this figure legend, the reader is referred to the web version of this article.)

to note that the addition of negative groups around the axial position will weaken the catalyst–cocatalyst interaction due to electrostatic repulsion between negatively charged groups. This observation reinforces the interpretation given for the steric model.

On the other hand, the blue contour showed in Fig. 4 corresponds to areas were an increase in positive charge will be beneficial for the polymer molecular weight. They are located around the *re* face, where chain transfer reactions occur as discussed above. An increase in positive charge can have an attractive effect for a cocatalyst molecule hindering the olefin uptake in this face, resulting in a higher molecular weight.

In summary, the steric and electrostatic models show similar pictures of the intermolecular interaction effect on the polymer molecular weight. The compound model resulting after combination of the two fields, steric and electrostatic, gives a final model with an r^2 correlation coefficient of 0.938 and a Standard Error of Estimate of 0.089 for three components. The composition was 75% steric and 25% electrostatic. Fig. 5 shows a plot of actual versus predicted values for the polymer molecular weight obtained with this model. We transformed to the logarithmic scale because the data distribution is more uniform, which is important for the statistical treatment.

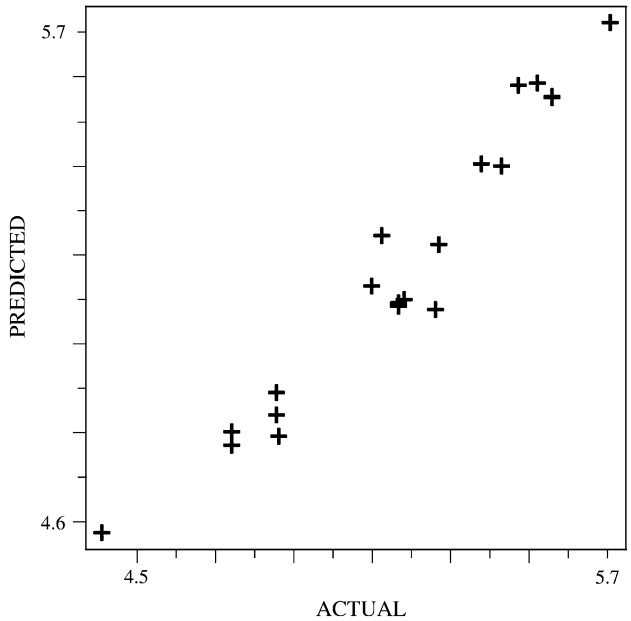

Fig. 5. Plot of predicted versus actual log(M_w) values.

Table 3
Experimental data from Ref. [28]

Catalyst	R1	R2	R3	M_w[a]
P1	2-^{t}Bu–Ph	2-^{t}Bu–Ph	Me	165 000
P2	2,5-^{t}Bu$_2$–Ph	2,5-^{t}Bu$_2$–Ph	Me	46 400
P3	2-CF$_3$–4-Cl–Ph	2–CF$_3$–4-Cl–Ph	Me	10 300
P4	2-CF$_3$–Ph	2-CF$_3$–Ph	Me	19 100
P5	2-CF$_3$–4-Br–Ph	2-CF$_3$–4-Br–Ph	Me	8900
P6	2,6-^{i}Pr$_2$–Ph	2,6-^{i}Pr$_2$–Ph	Me	48 400

Fe: 9 μmol; $T = 35$ °C; $P_{Eth.} = 1$ bar; [Al]/[Fe] = 400; toluene: 40 ml; $t_{Pol.} = 15$ min.
[a] g/mol.

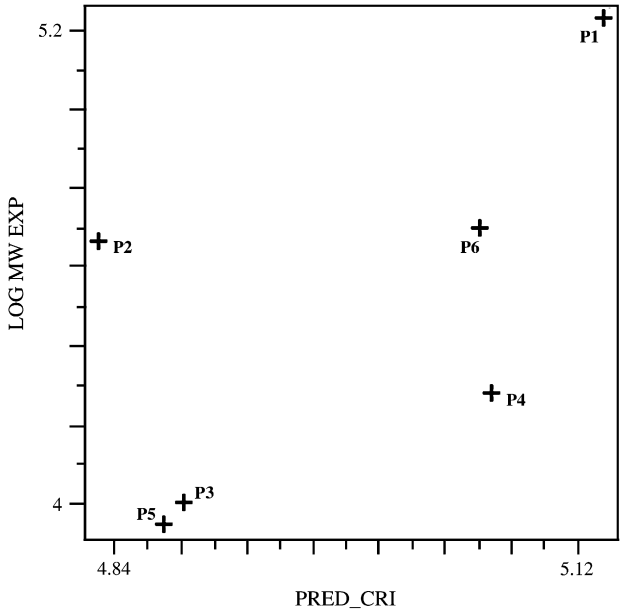

Fig. 6. Plot of actual versus predicted M_w values of the catalyst set reported in Ref. [28]. Data are in logarithmic scale.

3.3. Predictive capability

In addition to the informative capability of the QSAR models, these have the possibility of making predictions over compounds not considered in the training set, the set of compounds used to derive the model, or even not synthesized yet. Once the structure is optimised, conveniently aligned and the descriptors calculated, these are introduced into the QSAR equation and their properties were evaluated. The predictions made in this way have an error equal to the Standard Error of Prediction obtained after the cross-validation procedure.

We have performed predictions for the catalyst set reported by Pelascini et al. [21] and have shown in Table 3. Fig. 6 shows a graphical representation of predicted versus actual polymer molecular weight values. As can be seen, the predictions are good enough in five out of six compounds. Compound number **P2** is poorly predicted and we cannot provide a satisfactory explanation at this time. It is worth to mention that Pelascini and co-workers made their experiments in experimental conditions markedly different to those used in our training set, so it is necessary to consider relative values. However, the predicted values show the right ordering of molecular weights. This could be considered as a point in favour of the robustness of our model.

4. Conclusions

3D-QSAR models have been derived from olefin polymerisation catalysis obtained with bis(imino)pyridine Fe(II) complexes. We used the dichloride precursor structures because there is still uncertainty about the nature of the active species in this kind of catalysts. In spite of this assumption, we found a valid model which correlates the experimental polymer molecular weight with steric and electrostatic fields. This result proves the importance of intermolecular interactions most probably between catalyst and cocatalyst in the catalytic behaviour. At the same time, the QSAR model agrees satisfactorily well with other theoretical calculations as well as with experimental observations.

In particular, the steric effect seems to be the most important contribution, with about 75% of the total effect. The electrostatic model reinforces the interpretation of a catalyst–cocatalyst interaction affecting the polymerisation behaviour.

The positive steric effect is located around the *si* face where catalyst–cocatalyst interaction can compete against olefin complexation and insertion. In the same areas an increment of negative charge will be beneficial for higher molecular weight.

On the contrary, the steric contribution on the *re* face will enhance lower molecular weights. In these areas an increase in positive charge is correlated with higher molecular weight. This region is mainly associated with the polymerisation chain transfer reactions.

The fundamental methodologies used in 3D-QSAR are well established and can provide statistical robust models. However, some aspects need to be improved in order to get better results, as it is explained in what follows. One main concern is about the large number of descriptors that are used for the correlations. Possible solutions have been pointed out by Cruciani's group [39] regarding the application of variable selection methods in addition to the PLS methodology. Other improvements in the 3D-QSAR technique try to overcome the molecular alignment problem. The requirement is that all molecules in the set should be aligned in such a way that each point in the grid had the same meaning for each compound. This introduces some uncertainties which greatly affect the outcome of the final model. The implementation of auto-correlation and cross-correlation techniques simplifies this problem to the requirement of only one arbitrary point to be the common origin for all compounds. This point can be easily identified in the homogeneous catalysis case to be the metallic centre, for example.

In summary, we believe that chemometric tools should facilitate the rational design of polymerisation catalysts.

Acknowledgments

We gratefully acknowledge financial support from the Ministerio de Educación y Ciencia, Spain (Grant MAT2006-0400), CSIC (2005CL0049), the Comunidad de Madrid (S-0505/PPQ-0328). J. Ramos thanks CSIC for financial support through an I3P tenure track. The authors also acknowledge Centro Técnico de Informática (CTI-CSIC, Madrid, Spain), Centro de Supercomputación de Galicia (CESGA, Santiago de Compostela, Spain) and Centro de Investigaciones Energéticas, Medioambientales y Tecnológicas (CIEMAT, Madrid, Spain) for the use of their computational resources.

References

[1] Small BL, Brookhart M, Bennett AMA. J Am Chem Soc 1998;120:4049.
[2] Birtovsek GJP, Gibson V, Kimberley BS, Maddox PJ, McTavish SJ, Solan GA, et al. Chem Commun 1998;7:849–50.
[3] Gibson VC, Spitzmesser SK. Chem Rev 2003;103:283.
[4] Bianchini C, Giambastiani G, Rios IG, Mantovani G, Meli A, Segarra AM. Coord Chem Rev 2006;250:1391.
[5] Ittel SD, Johnson LK, Brookhart M. Chem Rev 2000;100:1169–203.
[6] Bohm LL. Angew Chem Int Ed 2003;42:5010.
[7] Fink G, Mulhaupt R, Brintzinger HH. Ziegler catalysts: recent scientific innovations and technological improvements. Berlin: Springer; 1995 and references therein.
[8] Kaul FAR, Puchta GT, Schneider H, Bielert F, Mihalios D, Herrmann WA. Organometallics 2002;21:74.
[9] Ray S, Galgali G, Lele A, Sivaram S. J Polym Sci 2004;43:304.
[10] Scott J, Gambarotta S, Korobkov I, Budzelaar PHM. J Am Chem Soc 2005;127:13019.
[11] Esteruelas MA, López AM, Méndez L, Oliván M, Oñate E. Organometallics 2003;22:395.
[12] Cámpora J, Naz AM, Palma P, Álvarez E, Reyes ML. Organometallics 2005;24:4878–81.
[13] Cámpora J, Conejo MM, Mereiter K, Palma P, Pérez C, Reyes ML, et al. J Organomet Chem 2003;683:220–39.
[14] Ivanchev SS, Yakimansky AV, Rogozin DG. Polymer 2004;45:6453.
[15] Paulino IS, Schuchardt U. J Mol Catal A 2004;211:55.
[16] Schmidt R, Welch MB, Knudsen RD, Gottfried S, Alt HG. J Mol Catal A 2004;222:9.
[17] Muir RM, Hansch C. Nature 1962;194:178.
[18] Kubinyi H, editor. 3D QSAR in drug design: theory methods and applications. Dordrecht: Kluwer/ESCOM; 2000.
[19] Cruz V, Ramos J, Muñoz-Escalona A, Lafuente P, Peña B, Martínez-Salazar J. Polymer 2004;45:2061.
[20] Cruz V, Ramos J, Martinez S, Muñoz-Escalona A, Martínez-Salazar J. Organometallics 2005;24:5095.
[21] Pelascini F, Peruch F, Lutz PJ, Wesolek M, Krees J. Eur Polym J 2005;41:1288.
[22] Becke AD. Phys Rev A 1998;38:3098.
[23] Hay PJ, Wadt WR. J Chem Phys 1985;82:299.
[24] Frisch MJ, Trucks GW, Schlegel HB, Scuseria GE, Robb MA, Cheeseman JR, et al. Gaussian 03 revision C.02. Wallingford, CT: Gaussian Inc.; 2004.
[25] Breneman CM, Wiberg KB. J Comput Chem 1990;11:361.
[26] Martin YC, Kim KH, Liu CT. In: Charton M, editor. Advances in quantitative structure–property relationships, vol. 1. Greenwich, CT: JAI Press; 1996. p. 1–52.
[27] Clark M, Cramer III RD, Van Opdenbosch N. J Comput Chem 1989; 10:982.
[28] Cramer III RD, Patterson DE, Bunce JD. J Am Chem Soc 1988;110:5959.
[29] SYBYL Molecular Modeling System Tripos Inc., 1699 S Hanley Rd, St Louis, MO 63144.
[30] Rännar S, Lindgren F, Geladi P, Wold S. J Chemom 1994;8:111.
[31] Wold S, Ruhe A, Wold H, Dunn WJ. SIAM J Sci Stat Comput 1984;5: 735.
[32] Cramer III RD, Bunce JD, Patterson DE, Frank IE. Quant Struct-Act Relat 1988;7:18.
[33] Clark M, Cramer III RD. Quant Struct-Act Relat 1993;12:137.
[34] Manz TA, Phomphrai K, Medvedev G, Krishnamurthy BB, Sharma S, Haq J, et al. J Am Chem Soc 2006;129:3776.
[35] Wade RC. In: Kubinyi H, editor. 3D QSAR in drug design: theory methods and applications. Dordrecht: Kluwer/ESCOM; 2000. p. 486–505.
[36] Cramer III RD, DePriest SA, Patterson DE, Hecht P. In: Kubinyi H, editor. 3D QSAR in drug design: theory methods and applications. Dordrecht: Kluwer/ESCOM; 2000. p. 443–85.
[37] Ramos J, Cruz V, Muñoz-Escalona A, Martinez-Salazar J. Polymer 2002;43:3635.
[38] Deng L, Margl P, Ziegler T. J Am Chem Soc 1999;121:6479.
[39] Cruciani G, Clementi S, Baroni M. In: Kubinyi H, editor. 3D QSAR in drug design: theory methods and applications. Dordrecht: Kluwer/ESCOM; 2000. p. 486–505.